

ARTICLE

Received 22 Jul 2016 | Accepted 9 Dec 2016 | Published 24 Feb 2017

DOI: 10.1038/ncomms14280

OPEN

Spectroelectrochemical analysis of the mechanism of (photo)electrochemical hydrogen evolution at a catalytic interface

Ernest Pastor^{1,†}, Florian Le Formal^{1,†}, Matthew T. Mayer², S. David Tilley^{2,†}, Laia Francàs¹, Camilo A. Mesa¹, Michael Grätzel² & James R. Durrant¹

Multi-electron heterogeneous catalysis is a pivotal element in the (photo)electrochemical generation of solar fuels. However, mechanistic studies of these systems are difficult to elucidate by means of electrochemical methods alone. Here we report a spectroelectrochemical analysis of hydrogen evolution on ruthenium oxide employed as an electrocatalyst and as part of a cuprous oxide-based photocathode. We use optical absorbance spectroscopy to quantify the densities of reduced ruthenium oxide species, and correlate these with current densities resulting from proton reduction. This enables us to compare directly the catalytic function of dark and light electrodes. We find that hydrogen evolution is second order in the density of active, doubly reduced species independent of whether these are generated by applied potential or light irradiation. Our observation of a second order rate law allows us to distinguish between the most common reaction paths and propose a mechanism involving the homolytic reductive elimination of hydrogen.

¹Department of Chemistry, Imperial College London, South Kensington Campus, London SW7 2AZ, UK. ²Institut des Sciences et Ingénierie Chimiques, Ecole Polytechnique Fédérale de Lausanne (EPFL), Laboratory of Photonics and Interfaces, Station 6, CH-1015 Lausanne, Switzerland. † Present addresses: Molecular Biophysics and Integrated Bioimaging Division, Lawrence Berkeley National Laboratory, One Cyclotron Road, Berkeley, California 94720, USA (E.P.); Institut des Sciences et Ingénierie Chimiques, Ecole Polytechnique Fédérale de Lausanne, Laboratory for Molecular Engineering of Optoelectronic Nanomaterials, Station 6, CH-1015 Lausanne, Switzerland (F.L.F.); Department of Chemistry, University of Zurich, Winterthurerstrasse 190, 8057 Zurich, Switzerland (S.D.T.). Correspondence and requests for materials should be addressed to J.R.D. (email: j.durrant@imperial.ac.uk).

Multi-electron heterogeneous redox catalysis is of increasing importance for the development of sustainable energy systems^{1,2}. These include for example the electrolysis or photoelectrolysis of water to release molecular hydrogen, and its utilization for electrical power generation, as well as strategies for CO₂ reduction^{3–5}. Determination of the mechanisms of such heterogeneous catalytic processes is often challenging. This is particularly the case for multi-electron processes, which may require the accumulation of multiple reduction or oxidizing species to drive the desired transformation⁶. The determination of the rate laws for such reactions in (photo)electrochemical systems, and in particular the dependence of the reaction rate upon the density of reduced/oxidized species, can provide powerful insights into the reaction mechanism. However, such rate law analyses are often difficult to elucidate from conventional electrochemical measurement strategies, except for ideal systems^{7,8}. In the study reported herein, we employ a combined optical/electrochemical approach to access and compare the rate law of proton reduction to H₂ under conditions of dark and light electrolysis.

Traditionally, precious metals that exhibit near ideal catalytic behaviour such as platinum have been employed as electrocatalysts for the hydrogen evolution reaction (HER)^{4,9}. Recently, a new generation of electrocatalysts based on nanostructured metal oxides and sulfides, as well as molecular catalysts, have emerged as potentially lower-cost alternatives^{3,10–17}. In this work, we have chosen to focus on a well-established HER electrocatalyst: RuO_x (ref. 18). This electrocatalyst is based upon a nanostructured, amorphous, highly porous RuO_x that herein is deposited onto FTO (fluorine-doped tin oxide) and onto a multilayer Cu₂O-based photoelectrode (Fig. 1). Such photocathodes, where the Cu₂O is protected against photocorrosion by thin Al:ZnO (AZO) and TiO₂ overlayers, have achieved remarkable solar-to-hydrogen yields and large (near 100%) faradaic efficiencies for solar-driven water splitting^{19–21}. This Cu₂O/AZO/TiO₂/RuO_x (referred herein as [Cu₂O]/RuO_x) assembly can be considered an example of a ‘buried junction’ photoelectrode, in which the generation and separation of photogenerated charges in the Cu₂O/AZO/TiO₂ layers is at least partially decoupled from the catalytic function by the catalyst overlayer. As such, these systems provide an attractive model for the study of the HER catalysis, as well as enabling a direct comparison of the catalytic function under conditions of dark electrochemical and irradiated photoelectrochemical proton reduction.

In this study, we are concerned with addressing the (photo)-electrocatalytic function of FTO/RuO_x and [Cu₂O]/RuO_x. In electrocatalytic systems, the first step toward the determination of a reaction mechanism is the analysis of its current/potential characteristics, often referred to, for metallic electrodes, as a Tafel analysis⁷. Such analyses are typically interpreted in terms of the

potential dependence of the free energy offset driving the reaction and can provide information about the nature of the rate-determining step⁷. However, for non-ideal semiconducting or metallic electrodes with multiple redox states, such as the RuO_x studied herein, the interpretation of Tafel analyses is non-trivial and is hampered by the presence of surface and/or intraband states²². For photoelectrochemical systems, the interpretation of current/potential data in terms of catalytic function is even more challenging due to the voltage dependence of electron/hole recombination, which can provide a further modulation of flux of charge carriers to the surface as a function of applied potential²³. As such, for many (photo)electrocatalytic systems, determination of rate laws for multi-redox reactions is a non-trivial challenge, with only limited studies reported in the literature to date.

The key challenge in undertaking purely rate law analyses of heterogeneous redox catalysis is the difficulty in determining the density of reducing species from electrochemical methods alone. In this study, we avoid this limitation by using optical absorbance difference spectroscopy to assay directly the densities of reduced RuO_x species under conditions of both electrochemical and photoelectrochemical proton reduction. This approach opens the possibility to study (photo)electrocatalysis in heterogeneous redox catalysts that are otherwise difficult to study by electrochemical methods alone. Recently, we have shown that it is possible to use such an optical assay to study the photoelectrochemical water oxidation on α -Fe₂O₃ and BiVO₄ photoanodes with high surface areas^{24,25}. However, it has not been applied to determine rate laws of electrocatalytic reactions. Employing this approach, we compare the behaviour of RuO_x when it is used as an electrocatalyst and as a part of a Cu₂O-based multi-junction photocathode. Taking advantage of the high internal surface area of the RuO_x, we demonstrate that we are able to monitor separately the densities of singly and doubly reduced RuO_x, and how these densities correlate with the current density for proton reduction. These measurements are used to determine the rate law for both electrochemical and photoelectrochemical proton reduction and thus gain insights into the catalytic mechanism of the HER.

Results

Current/potential characteristics. We start by comparing the current/potential (*J*-*E*) characteristics of the RuO_x electrocatalyst in the dark (on FTO) and on the multilayer [Cu₂O] photocathode under irradiation (Fig. 2a). The negative currents observed under reducing bias for both systems are assigned to the

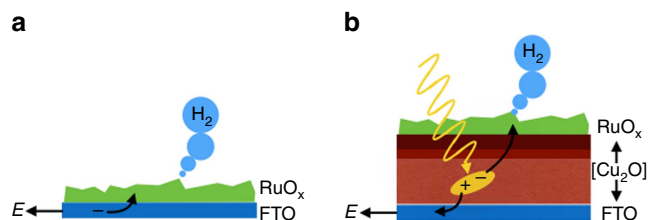


Figure 1 | Schematic representation of the dark and light electrocatalytic systems. (a) RuO_x/FTO cathode and (b) FTO/Cu₂O/AZO/TiO₂/RuO_x photocathode. The diagram is not scaled.

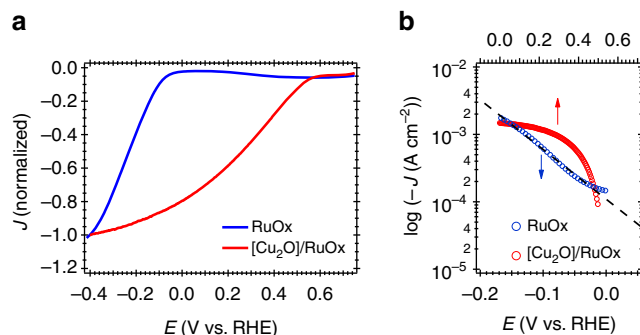


Figure 2 | *J*-*E* behaviour of the dark electrocatalyst and the illuminated photocathode. (a) *J*-*E* characteristics normalized for clarity at an applied potential where HER occurs in both systems and (b) *J*-*E* characteristics represented as log [−*J* or −*J*^{ph}] versus *E*. The samples were measured in a pH = 5 phosphate-sulfate electrolyte.

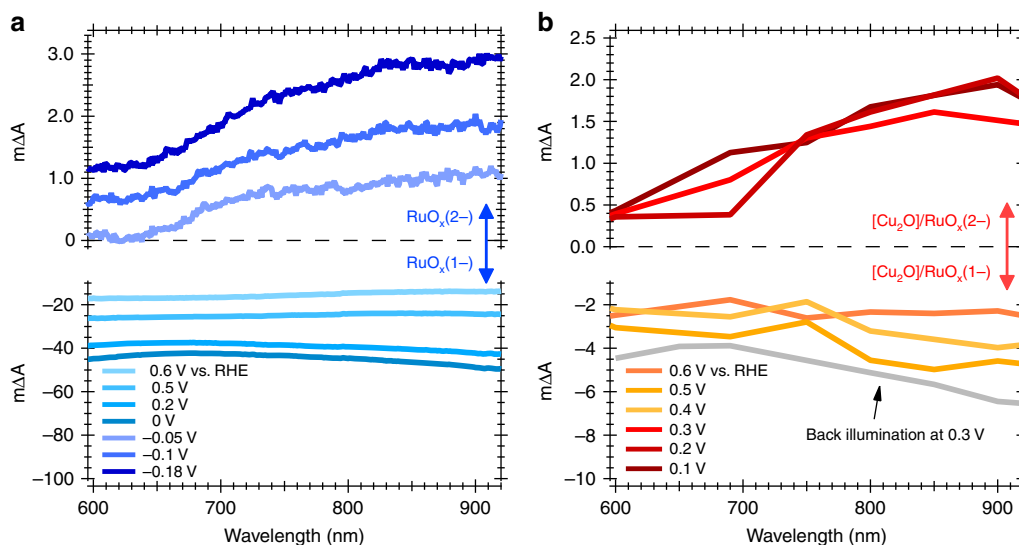


Figure 3 | Spectroelectrochemical spectra at different applied potentials. Spectra showing the changes in absorbance ($\Delta A \times 10^{-3}$) when RuO_x (a) acts as a dark electrocatalyst and (b) is part of a $[\text{Cu}_2\text{O}]$ photocathode under irradiation. For the lower box in a, ΔA is plotted relative to the absorbance spectrum at open circuit potential (OCP = 0.78 V); for the upper box, showing ΔA spectra at potentials negative of the hydrogen reduction current onset potential ($E_{\text{onset}} = 0$ V versus RHE), the spectra are plotted relative to that at this onset potential. For the $[\text{Cu}_2\text{O}]/\text{RuO}_x$ photocathode (b), at all potentials ΔA is plotted as the difference between light on and light off. For reference, the ΔA with respect to the absorbance at OCP and the simultaneously measured currents for all applied potentials are shown in Supplementary Figs 3 and 4. For both device types, the negative ΔA signals observed for $E > E_{\text{onset}}$ are assigned to RuO_x reduction to $\text{RuO}_x(-1)$, and the positive ΔA signals observed for $E < E_{\text{onset}}$ are assigned to the further reduction to $\text{RuO}_x(-2)$ species. For (b) the irradiation conditions were ~ 5 -6 s (25 s for back irradiation), 365 nm illumination ($\sim 1.5 \text{ mW cm}^{-2}$). See Methods for experimental details.

HER deriving from proton reduction¹⁹. The J - E response reveals an approximate 0.5 V difference in the onset of proton reduction catalysis between the electrocatalytic ($E_{\text{onset}} \sim 0$ V versus RHE) and the photocatalytic systems ($E_{\text{onset}} \sim 0.5$ V versus RHE) in agreement with the photovoltage provided by the buried p- $\text{Cu}_2\text{O}/\text{n-Al:ZnO}$ junction²⁶. It is apparent that the shape of the J - E curve of the dark and light-driven systems are qualitatively different despite tracking the same catalytic reaction (HER on RuO_x); in particular, the current onset is much sharper for the dark, electrochemically driven reaction. In addition to this, we also observe a small negative current at potentials positive to E_{onset} for both systems. This is also present as a quasi-reversible wave in cyclic voltammogram of RuO_x (Supplementary Fig. 1), and has previously been assigned to the first reduction of the catalyst from RuO_2 , most probably to $\text{Ru}(\text{OH})_3$, (herein referred for simplicity as $\text{RuO}_x(1-)$)^{27,28}.

Figure 2b shows the J - E behaviour plotted on a log/linear graph as typically employed for analyses of catalytic function. The dark electrocatalytic current density of RuO_x displays near-linear dependence of $\log[-J]$ versus E , over the limited potential range shown, with a Tafel slope of 140 mV dec^{-1} . As discussed above and elsewhere, the RuO_x studied herein consists of a porous, non-stoichiometric electrocatalytic layer with multiple redox/protonation states, therefore, the direct interpretation of this Tafel slope is complex^{29,30}. Moreover, the current density of $[\text{Cu}_2\text{O}]/\text{RuO}_x$ does not show a logarithmic dependence on the applied potential, assigned below to the potential dependence of photoinduced charge recombination. As such, we focus herein on an alternative spectroelectrochemical analysis of these (photo)electrodes.

A key difference in the electrochemical response between electrocatalysts and photoelectrocatalysts is the impact of potential-dependent charge separation or recombination in light-driven systems^{23,31}. Such recombination losses can be

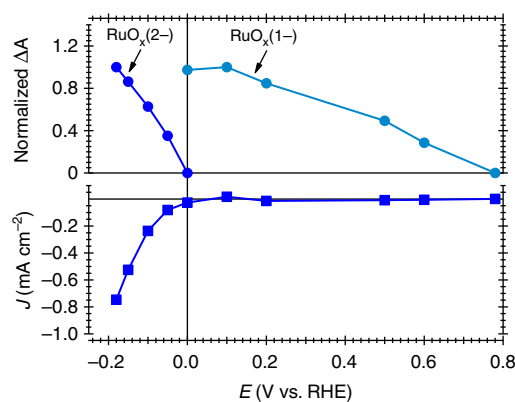


Figure 4 | Correlation between the changes in absorbance and current.

The ΔA was calculated as an average of the optical signal between 850 and 900 nm and represented in a normalized scale for clarity. The steady state current density was calculated as the average current measured within 300-350 s (see Supplementary Fig. 4).

observed in the photocurrent (J^{ph}) response of the photocathode as sharp cathodic and anodic photocurrent spikes when the light is turned on and off, respectively (Supplementary Fig. 2). Analogous current transients have been reported in other photoelectrodes, and have been assigned to the recombination of charges accumulated at the semiconductor/liquid interface competing with the catalytic reaction^{23,32}. The magnitude of these current transients is reduced upon the application of stronger negative potentials, indicating that these partially suppress recombination losses. The surface recombination current transients are even more dominant for the $[\text{Cu}_2\text{O}]$ photocathode alone in the absence of RuO_x , indicating that the deposition of

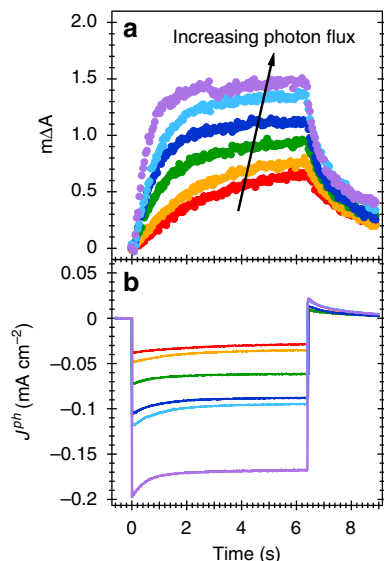


Figure 5 | Absorbance and photocurrent changes under conditions of HER. (a) Time-dependent photoinduced absorbance changes of the photocathode upon 365 nm light illumination at different photon fluxes ($0.5\text{--}1.5\text{ mW cm}^{-2}$) at a fixed applied potential of $0.1\text{ V}_{\text{RHE}}$ and (b) the photocurrent measured simultaneously.

RuO_x results in the partial suppression of these recombination losses. As such, it is apparent that for $[\text{Cu}_2\text{O}]/\text{RuO}_x$, the $J\text{-}E$ behaviour shown in Fig. 2 is primarily determined by the potential dependence of recombination losses, and therefore cannot be used as direct assay of the catalytic behaviour of the RuO_x layer in this system.

Spectroelectrochemical characteristics. We turn now to an optical spectroscopy investigation of the RuO_x functioning as a dark HER electrocatalyst on FTO. Figure 3a shows the spectroelectrochemical data for this electrode, plotted as absorbance difference (ΔA) against wavelength at different applied potentials. At potentials negative of the electrode open circuit potential (OCP , $0.78\text{ V}_{\text{RHE}}$), a broad negative change in absorbance (bleaching of the absorbance at OCP) is observed across the visible/near-IR region. This loss in absorbance increases with increasing reducing potential until 0 V_{RHE} , which corresponds to the onset of the proton reduction electrocatalytic wave, E_{onset} . Further increase in applied potential negative of 0 V_{RHE} results in appearance of a new, positive change in absorbance with respect to E_{onset} , with increasing amplitude toward the near-IR ($\sim 900\text{ nm}$). Following our discussion of the electrochemical data above, we assign the negative absorbance at potentials between OCP and E_{onset} to the reduction of RuO_x to its singly reduced species, $\text{RuO}_x(1-)$, and the positive absorbance at potentials negative of E_{onset} to formation of further reduced catalytic species herein referred as $\text{RuO}_x(2-)$. Comparison of the amplitudes of these two optical absorbance signals with the steady state catalytic current assigned to the HER suggests that there is correlation between the second reduction of the electrocatalyst to $\text{RuO}_x(2-)$ and the electrocatalysed HER (Fig. 4). Our optical data indicate that formation of $\text{RuO}_x(2-)$ is only observed once the first reduction of the electrocatalyst to $\text{RuO}_x(1-)$ is saturated (see Fig. 4 and also Supplementary Fig. 3). Following literature data, the reduction of RuO_x to $\text{RuO}_x(1-)$ is most probably associated with Ru^{IV} reduction to Ru^{III} hydroxo species coupled with a lattice expansion^{27,28,33}, and the second reduction to

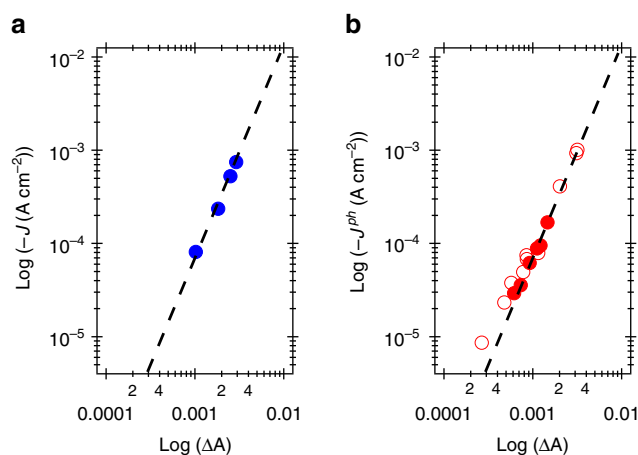


Figure 6 | Relationship between (photo)current and absorbance changes.

(a) Current-absorbance characteristics of the RuO_x electrocatalyst represented as the $\log[-J]$ versus the absorbance of the catalytic RuO_x species at different applied potentials (-0.05 to -0.2 V versus RHE).

(b) Photocurrent-absorbance characteristics of the photocathode represented as the $\log[-J^{\text{ph}}]$ versus the photoinduced absorbance of the catalytic RuO_x species generated at 0.1 V versus RHE upon 365 nm illumination at different photon fluxes (~ 0.5 to 1.5 mW cm^{-2}). The regression of $\log[-J]$ versus $\log[\Delta A]$ yielded slopes of 2.1 ± 0.1 (correlation coefficient, $R = 0.997$) for the electrocatalyst. For the photocatalyst two sets of data are shown, collected with (empty circles, see Supplementary Fig. 8) and without (solid circles, see Fig. 5) the addition of 0.01 M surfactant (Triton X-100) used to promote facile bubble release. The independent data sets have been normalized to be plotted in the same graph. The regression of $\log[-J^{\text{ph}}]$ versus $\log[\Delta A]$ of each dataset yielded identical slopes of 1.9 ± 0.1 ($R = 0.992$).

$\text{RuO}_x(2-)$ is probably associated with formation of ruthenium hydrides (see ‘Discussion’ section), although we note that the specific nature of these states is not the primary focus of the study herein.

Next we focus on the spectroelectrochemical analysis of $[\text{Cu}_2\text{O}]/\text{RuO}_x$, enabled by its recent adaptation as a transparent photocathode for tandem operation³⁴. In this case, current generation, and therefore RuO_x reduction, is both light and voltage dependent. We focus on the change in the absorbance (ΔA) induced by UV (365 nm) irradiation, measured at different applied potentials (Fig. 3b), with control data in the absence of Cu_2O showing negligible signals (Supplementary Fig. 5). The resulting data show qualitative similarities to the dark spectroelectrochemical of RuO_x alone (Fig. 3a). At potentials positive of the onset of photocurrent ($>0.4\text{ V}_{\text{RHE}}$), a broad negative change in absorbance is observed; for more negative potentials, where HER photocurrent is monitored, a positive absorbance change is observed. The striking similarity between the absorbance changes induced electrochemically for bare RuO_x and photoelectrochemically for $[\text{Cu}_2\text{O}]/\text{RuO}_x$ suggest that in both cases we are primarily monitoring the same species of $\text{RuO}_x(1-)$ and $\text{RuO}_x(2-)$. Further evidence that RuO_x dominates the optical signals is found upon back illumination of $[\text{Cu}_2\text{O}]/\text{RuO}_x$ under moderate bias ($0.3\text{ V}_{\text{RHE}}$). Under these conditions in which negligible photocurrent is obtained (Supplementary Fig. 6), only the negative absorbance change assigned to singly reduced, non-catalytically active $\text{RuO}_x(1-)$ is monitored (Fig. 3b).

We now consider the quantitative correlation between the density of $\text{RuO}_x(2-)$ species and the HER current. For dark electrocatalysis, this is provided by the optical

and current density data as a function of applied potential (Fig. 4). However, for the photocathode, the potential dependence of recombination losses complicates the interpretation of the equivalent data. We avoid this by measuring the change in absorbance upon light pulses of different intensities at a fixed, moderate reducing potential ($0.1 V_{\text{RHE}}$). Figure 5 shows the absorbance change at 900 nm and the associated photocurrent measured as a response to 6 s light pulses. As expected, an increase in the light intensity results in larger steady state photocurrents and larger absorbance changes corresponding to the accumulation of more catalytic $\text{RuO}_x(2-)$ species. The decay of the absorbance signal following light off is assigned primarily to the decay of $\text{RuO}_x(2-)$ species due to proton reduction, indicating a 0.1s–1s timescale for this reaction (see also Supplementary Fig. 7).

Rate law analysis. Figure 6 summarizes our different experimental assays of the catalytic function of RuO_x and $[\text{Cu}_2\text{O}]/\text{RuO}_x$ plotted as the $\log[-J]$ (or $-J^{ph}$) against the optical absorbance increase ($\log[\Delta A]$) measured at 900 nm, (that is, $\text{RuO}_x(2-)$). For RuO_x , this log/log representation of the current flow shows a linear dependence with a slope of 2.1 (Fig. 6a). For $[\text{Cu}_2\text{O}]/\text{RuO}_x$, the photocurrent also shows a similar linear dependence on the change in absorbance with a gradient of 1.9 (Fig. 6b). These data provide a clear indication that for both systems, the catalytic current is proportional to approximately the square of the density of $\text{RuO}_x(2-)$. Furthermore, the two plots overlay almost exactly, indicating that for both systems, the HER current density depends indistinguishably upon the density of $\text{RuO}_x(2-)$. This agreement is particularly striking given the different experimental methods employed—analysis of the dark current as a function of applied bias and of the photocurrent as a function light intensity, and provides confirmation of the validity of the experimental approaches employed herein.

Discussion

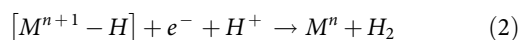
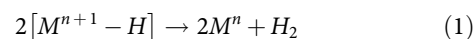
The experimental approach employed herein is based upon the use of an optical assay of the density of doubly reduced RuO_x species ($\text{RuO}_x(2-)$) and its correlation with electrocatalytic and photocatalytic proton reduction to hydrogen on FTO/ RuO_x and $[\text{Cu}_2\text{O}]/\text{RuO}_x$, respectively. For both systems, this optical absorbance signal is only observed for applied potentials negative of the onset of catalytic HER current; for less reducing potentials, a broad, negative absorbance change is observed, assigned to the single reduction of RuO_x to a pre-catalytic $\text{RuO}_x(1-)$ state. Our approach therefore provides a direct way to relate the dependence of the (photo)current to $\text{RuO}_x(2-)$. Strikingly, our plots of $\log[-J]$ versus $\log[\Delta A]$ for electrochemical and photoelectrochemical proton reduction reveal an identical dependence of the current on $\text{RuO}_x(2-)$. This observation contrasts with the different J - E responses of these systems (Fig. 2). This difference in J - E between the electrocatalytic and photocatalytic systems results primarily from the voltage dependence of photoinduced charge separation and recombination in the $[\text{Cu}_2\text{O}]/\text{RuO}_x$ photocathode.

For the dark RuO_x electrocatalyst, the electrochemical J - E response shown in Fig. 2b shows a linear relationship between $\log[-J]$ and E , typical of many electrochemical reactions^{22,35,36}. For metals, such behaviour is usually interpreted in terms of differences in reaction overpotential as a function of applied potential. In contrast, our optical assay of $\text{RuO}_x(2-)$ reveals that the concentration of this catalytically active species increases approximately linearly with applied

potential above the E_{onset} (see Fig. 4), clearly distinct from ideal metallic or semiconductor behaviour. Such non-ideal behaviour, which may result from multiple reaction intermediates, the protonation of the surface states or other origins of state inhomogeneity³⁷, makes direct interpretation of electrochemical data alone very challenging. In contrast, our spectroelectrochemical analysis allows us to correlate the observed (photo)electrocatalytic HER current with the density of reduced, catalytic $\text{RuO}_x(2-)$, facilitating analysis of RuO_x function. Moreover, this analysis allows us to compare directly the light and dark electrochemistry bypassing the effect of carrier recombination in the J^{ph} - E response.

Our analysis of the dark RuO_x/FTO and photo-driven $[\text{Cu}_2\text{O}]/\text{RuO}_x$ systems under steady state conditions (Fig. 6) reveals both systems exhibit the same second-order dependence of HER current density upon $\text{RuO}_x(2-)$. This observation provides evidence that for this catalyst, the catalytic function is independent of substrate (that is, FTO or $\text{Cu}_2\text{O}/\text{AZO}/\text{TiO}_2$ -buried junction), of the mechanism driving the reaction (that is, electrochemical or photoelectrochemical) and of the means by which the density of $\text{RuO}_x(2-)$ is varied (that is, variation of applied potential or light intensity). Furthermore, the analysis indicates that in terms of catalytic function, the $[\text{Cu}_2\text{O}]/\text{RuO}_x$ can indeed be considered a buried junction device, where the catalytic function of the RuO_x is independent of the $[\text{Cu}_2\text{O}]$ underlayers. However, we note that the RuO_x also appears to have an additional function reducing charge recombination losses in the photocathode (Supplementary Fig. 2), such that function of the $\text{Cu}_2\text{O}/\text{AZO}/\text{TiO}_2$ junction is dependent upon the presence of the surface catalytic layer.

We consider now the implications of our results for the mechanism of the HER on RuO_x . The HER is often described to occur through a homolytic or a heterolytic path involving the formation of metal-hydride intermediates ($[\text{M}^{n+1}-\text{H}]$)^{18,38–40}. In the homolytic mechanism, the H_2 evolution step involves the interaction of two hydrides and the reductive elimination of H_2 (equation 1). On the other hand, in the heterolytic mechanisms, the hydride intermediate undergoes further reduction and protonation to generate H_2 (equation 2).



Previous studies of HER on RuO_2 have proposed a heterolytic mechanism on the basis of electrochemical Tafel analyses^{18,41,42}. However, other literature on electrocatalytic proton reduction on other electrocatalysts has tended to favour homolytic reaction pathways^{30,43}. The interpretation of analyses that rely exclusively on J - E characteristics is complex for systems with multiple redox intermediates, where the surface behaviour differs from that of a metal, as discussed above³⁷. In contrast, our electro-optical analyses of the rate-determining step of the dark electrochemical and light-driven photoelectrochemical HER on RuO_x reveals a second-order reaction with respect to the concentration of $\text{RuO}_x(2-)$. Such behaviour is characteristic of bimolecular processes and thus is indicative of a homolytic rather than heterolytic reaction path involving two $\text{RuO}_x(2-)$ species.

On the basis of this observation and previous literature, we propose a tentative mechanism in which initially, before E_{onset} , RuO_x ($x \leq 2$) undergoes a one electron reduction forming $\text{Ru}(\text{OH})_3$ ($\text{RuO}_x(1-)$), as previously characterized^{27,28,33}. Following this pre-catalytic step, a further reduction of $\text{Ru}(\text{OH})_3$ occurs to generate the active species herein referred as $\text{RuO}_x(2-)$. Finally, two active species undergo the reductive elimination of H_2 regenerating the pre-catalytic state (equation 2). The specific nature of $\text{RuO}_x(2-)$ is beyond the

scope of this paper; however, on the basis of the previously suggested mechanisms, we hypothesize this to be a hydride-like species. We note that detailed studies on the nature of the pre-catalytic and catalytic species observed in our system are required to elucidate the mechanism unequivocally. However, our electro-optical analysis provides a powerful tool to discern between the two most common reaction mechanisms and thus to identify a potential mechanistic route.

In conclusion, in this work, we have presented a combined spectroscopic/electrochemical methodology that allows us to assay the densities of redox species directly under conditions of proton reduction and to correlate these with the respective current densities. This methodology thus enables direct access to the rate law for both electrochemical and photoelectrochemical proton reduction, even for non-ideal surfaces with multiple redox states. Our measurements reveal that HER on RuO_x takes place on the 0.1s–1s timescale via a bimolecular mechanism involving two doubly reduced RuO_x species. We find that the RuO_x behaves indistinguishably when employed as an electrocatalyst on FTO or as part of a photoelectrode, with the rate of hydrogen evolution primarily being determined by the density of doubly reduced RuO_x species, independent of whether these species are generated by applied potential or light irradiation. This spectroelectrochemical methodology allows us to simultaneously harness the advantages of electrochemical and optical methods to study the rate law of non-ideal (photo)electrodes. Provided that the catalytic active species can be optically resolved, this approach has the potential to be applicable to other heterogeneous systems. Our studies are ongoing to investigate the wider applicability of our analysis including consideration of other oxide and nitride electrodes and hybrid inorganic/molecular systems.

Methods

Photocathode preparation. The transparent [Cu₂O]/RuO_x photocathode was prepared as reported previously³⁴. In summary, electrodes of fluorine-doped tin oxide on glass (FTO, TEC-15, NSG glass) were treated by brief sputter depositions of Au to yield suitable transparent substrates for the electrodeposition of Cu₂O, which was performed from a basic solution of lactate-stabilized copper sulfate²⁰. A deposition time of 100 min was used, yielding a Cu₂O layer thickness of ~500 nm. This was directly followed by atomic layer deposition of Al:ZnO (20 nm) and TiO₂ (100 nm) (Savannah 100, Cambridge Nanotech).

RuO_x (photo)electrodeposition. Samples (Cu₂O photocathode and bare FTO) were passivated by opaque epoxy (Loctite Hysol 9461) to define the active area, then were immersed into aqueous solutions of 1.3 mM KRuO₄ for galvanostatic electrodeposition of RuO_x (ref. 19). A current density of $-28.3 \mu\text{A cm}^{-2}$ was applied to each for 900 s. For the case of the photocathode, the device was illuminated by a solar simulator (1-sun intensity) to facilitate cathodic charge flow. The resulting ~30 nm thick samples were amorphous and highly porous as previously characterized^{19,34}. The samples were then ready for electrochemical testing.

Electrochemical set-up. All measurements have been performed in a three-electrode photoelectrochemical cell. The cell was filled with ~10 ml of a combined phosphate 0.1-Na₂SO₄ 0.4 M electrolyte adjusted at pH = 5 and platinum gauze was used as a counter electrode. The pH was controlled through the experiment with a Hanna HI 83141 pH-meter. The sample was irradiated at the electrolyte/semiconductor interface. Potentials were applied against a silver/silver chloride reference electrode, with saturated KCl solution and converted to potentials against the reversible hydrogen potential (E_{RHE}) according to the Nernst equation.

(Photo)electrochemical set-up. Photoinduced absorption and transient photocurrent were measured simultaneously as previously described²⁴. The samples were irradiated with light pulses produced with the 365 nm LED (5–6 s on/5–6 s off). The probe light source was a tungsten lamp (Bentham IL1 tungsten lamp), and the probe wavelength was selected using a monochromator placed before the sample. Several long-pass and band-pass filters (Comar Instruments) were used to attenuate the pump (LED) light arriving at the detector. Spectroelectrochemistry measurements as a function of applied potential were performed by fitting the photoelectrochemical cell in a Perkin Elmer (Lambda 25) spectrometer. Potentials

were controlled using a PGSTAT101 potentiostat (Metrohm Autolab). The absorbances were measured when the current density attained steady state.

Data availability. The data of this study is available upon request.

References

- Wang, Q. *et al.* Scalable water splitting on particulate photocatalyst sheets with a solar-to-hydrogen energy conversion efficiency exceeding 1%. *Nat. Mater.* **15**, 1–3 (2016).
- Haro, M. *et al.* Toward stable solar hydrogen generation using organic photoelectrochemical cells. *J. Phys. Chem. C* **119**, 6488–6494 (2015).
- Willkomm, J. *et al.* Dye-sensitized semiconductors modified with molecular catalysts for light-driven H₂ production. *Chem. Soc. Rev.* **45**, 9–23 (2016).
- Cook, T. R. *et al.* Solar energy supply and storage for the legacy and nonlegacy worlds. *Chem. Rev.* **110**, 6474–6502 (2010).
- Windle, C. D. *et al.* Improving the photocatalytic reduction of CO₂ to CO through immobilisation of a molecular Re catalyst on TiO₂. *Chem. A Eur. J.* **21**, 3746–3754 (2015).
- Hammarström, L. Accumulative charge separation for solar fuels production: coupling light-induced single electron transfer to multielectron catalysis. *Acc. Chem. Res.* **48**, 840–850 (2015).
- Shinagawa, T., Garcia-Esparza, A. T. & Takanabe, K. Insight on Tafel slopes from a microkinetic analysis of aqueous electrocatalysis for energy conversion. *Sci. Rep.* **5**, 13801 (2015).
- Holewinski, A. & Linic, S. Elementary mechanisms in electrocatalysis: revisiting the ORR Tafel slope. *J. Electrochem. Soc.* **159**, H864–H870 (2012).
- Trasatti, S. Work function, electronegativity, and electrochemical behaviour of metals: III. Electrolytic hydrogen evolution in acid solutions. *J. Electroanal. Chem. Interfacial Electrochem.* **39**, 163–184 (1972).
- Guijarro, N., Prévot, M. S. & Sivula, K. Surface modification of semiconductor photoelectrodes. *Phys. Chem. Chem. Phys.* **17**, 15655–15674 (2015).
- Berardi, S. *et al.* Molecular artificial photosynthesis. *Chem. Soc. Rev.* **43**, 7501–7519 (2014).
- Kaeffer, N., Chavarot-Kerlidou, M. & Artero, V. Hydrogen evolution catalyzed by cobalt diimine-dioxime complexes. *Acc. Chem. Res.* **48**, 1286–1295 (2015).
- Lassalle-Kaiser, B. *et al.* Evidence from *in situ* X-ray absorption spectroscopy for the involvement of terminal disulfide in the reduction of protons by an amorphous molybdenum sulfide electrocatalyst. *J. Am. Chem. Soc.* **137**, 314–321 (2015).
- Vesborg, P. C. K., Seger, B. & Chorkendorff, I. Recent development in hydrogen evolution reaction catalysts and their practical implementation. *J. Phys. Chem. Lett.* **6**, 951–957 (2015).
- Helm, M. L., Stewart, M. P., Bullock, R. M., DuBois, M. R. & DuBois, D. L. A synthetic nickel electrocatalyst with a turnover frequency above 100,000 s⁻¹ for H₂ production. *Science* **333**, 863–866 (2011).
- Zheng, Y. *et al.* Hydrogen evolution by a metal-free electrocatalyst. *Nat. Commun.* **5**, 1–8 (2014).
- Merki, D. & Hu, X. Recent developments of molybdenum and tungsten sulfides as hydrogen evolution catalysts. *Energy Environ. Sci.* **4**, 3878 (2011).
- Over, H. Surface chemistry of ruthenium dioxide in heterogeneous catalysis and electrocatalysis: from fundamental to applied research. *Chem. Rev.* **112**, 3356–3426 (2012).
- Tilley, S. D., Schreier, M., Azevedo, J., Stefiik, M. & Graetzel, M. Ruthenium oxide hydrogen evolution catalysis on composite cuprous oxide water-splitting photocathodes. *Adv. Funct. Mater.* **24**, 303–311 (2014).
- Paracchino, A., Laporte, V., Sivula, K., Grätzel, M. & Thimsen, E. Highly active oxide photocathode for photoelectrochemical water reduction. *Nat. Mater.* **10**, 456–461 (2011).
- Morales-Guio, C. G., Tilley, S. D., Vrubel, H., Grätzel, M. & Hu, X. Hydrogen evolution from a copper(I) oxide photocathode coated with an amorphous molybdenum sulphide catalyst. *Nat. Commun.* **5**, 3059 (2014).
- Tan, M. X. *et al.* in *Progress in Inorganic Chemistry* Vol. 41 (ed. Karlin, K. D.) Ch. 2 (Wiley & Sons, 1994).
- Le Formal, F. *et al.* Back electron-hole recombination in hematite photoanodes for water splitting. *J. Am. Chem. Soc.* **136**, 2564–2574 (2014).
- Le Formal, F. *et al.* Rate law analysis of water oxidation on a hematite surface. *J. Am. Chem. Soc.* **137**, 6629–6637 (2015).
- Ma, Y., Kafizas, A., Pendlebury, S. R., Le Formal, F. & Durrant, J. R. Photoinduced absorption spectroscopy of CoPi on BiVO₄: the function of CoPi during water oxidation. *Adv. Funct. Mater.* **26**, 4951–4960 (2016).
- Paracchino, A. *et al.* Ultrathin films on copper(i) oxide water splitting photocathodes: a study on performance and stability. *Energy Environ. Sci.* **5**, 8673 (2012).
- Juodkazytė, J., Vilkauskaitė, R., Šebeka, B. & Juodkaziis, K. Difference between surface electrochemistry of ruthenium and RuO₂ electrodes. *Trans. IMF* **85**, 194–201 (2007).
- Sugawara, Y., Yadav, A. P., Nishikata, A. & Tsuru, T. EQCM study on dissolution of ruthenium in sulfuric acid. *J. Electrochem. Soc.* **155**, B897 (2008).

29. Fajardo, A. M. & Lewis, N. S. Free-energy dependence of electron-transfer rate constants at Si/liquid interfaces. *J. Phys. Chem. B* **101**, 11136–11151 (1997).
30. Kibler, L. A. Hydrogen electrocatalysis. *ChemPhysChem* **7**, 985–991 (2006).
31. Le Formal, F., Sivula, K. & Grätzel, M. The transient photocurrent and photovoltage behavior of a hematite photoanode under working conditions and the influence of surface treatments. *J. Phys. Chem. C* **116**, 26707–26720 (2012).
32. Peter, L. M., Wijayantha, K. G. U. & Tahir, A. A. Kinetics of light-driven oxygen evolution at α -Fe₂O₃ electrodes. *Faraday Discuss.* **155**, 309–322 (2012).
33. Karlsson, R. K. B., Cornell, A. & Pettersson, L. G. M. Structural changes in RuO₂ during electrochemical hydrogen evolution. *J. Phys. Chem. C* **120**, 7094–7102 (2016).
34. Dias, P. *et al.* Transparent cuprous oxide photocathode enabling a stacked tandem cell for unbiased water splitting. *Adv. Energy Mater.* **5**, 1501537 (2015).
35. Fajardo, A. M. & Lewis, N. S. Rate constants for charge transfer across semiconductor-liquid interfaces. *Science* **274**, 969–972, 1996).
36. Hamann, T. W., Gstrein, F., Brunshwig, B. S. & Lewis, N. S. Measurement of the free-energy dependence of interfacial charge-transfer rate constants using ZnO/H₂O semiconductor/liquid contacts. *J. Am. Chem. Soc.* **127**, 7815–7824 (2005).
37. Boodts, J. C. F. & Trasatti, S. Hydrogen evolution on iridium oxide cathodes. *J. Appl. Electrochem.* **19**, 255–262 (1989).
38. Gimbert-Suriñach, C. *et al.* Efficient and limiting reactions in aqueous light-induced hydrogen evolution systems using molecular catalysts and quantum dots. *J. Am. Chem. Soc.* **136**, 7655–7661 (2014).
39. Thoi, V. S., Sun, Y., Long, J. R. & Chang, C. J. Complexes of earth-abundant metals for catalytic electrochemical hydrogen generation under aqueous conditions. *Chem. Soc. Rev.* **42**, 2388–2400 (2013).
40. Elgrishi, N., McCarthy, B. D., Rountree, E. S. & Dempsey, J. L. Reaction pathways of hydrogen-evolving electrocatalysts: electrochemical and spectroscopic studies of proton-coupled electron transfer processes. *ACS Catal.* **6**, 3644–3659 (2016).
41. Kodintsev, I. M. & Trasatti, S. Electrocatalysis of H₂ evolution on RuO₂ + IrO₂ mixed oxide electrodes. *Electrochim. Acta* **39**, 1803–1808 (1994).
42. Chen, L. Kinetics of the hydrogen evolution reaction on RuO₂ and IrO₂ oxide electrodes in H₂SO₄ solution: an AC impedance study. *J. Electrochem. Soc.* **143**, 3576 (1996).
43. Nørskov, J. K. *et al.* Trends in the exchange current for hydrogen evolution. *J. Electrochem. Soc.* **152**, J23 (2005).

Acknowledgements

We gratefully acknowledge financial support from the European Research Council (project Intersolar 291482), Swiss National Science Foundation (project: 140709), Swiss Federal Office for Energy (project: PECHouse 3, contract number SI/500090–03). L.F. thanks the EU for a Marie Curie fellowship (658270). E.P. also thanks the EPSRC for a DTP scholarship.

Author contributions

E.P. and F.L.F. developed the experimental set-up and conducted the experiments. J.R.D. designed the experiments. M.T.M. and S.D.T. prepared the samples. E.P. and J.R.D. wrote the paper, with the help of F.L.F., M.T.M., S.D.T., L.F., C.A.M. and M.G.

Additional information

Supplementary Information accompanies this paper at <http://www.nature.com/naturecommunications>

Competing financial interests: The authors declare no competing financial interests.

Reprints and permission information is available online at <http://npg.nature.com/reprintsandpermissions/>

How to cite this article: Pastor, E. *et al.* Spectroelectrochemical analysis of the mechanism of (photo)electrochemical hydrogen evolution at a catalytic interface. *Nat. Commun.* **8**, 14280 doi: 10.1038/ncomms14280 (2017).

Publisher's note: Springer Nature remains neutral with regard to jurisdictional claims in published maps and institutional affiliations.



This work is licensed under a Creative Commons Attribution 4.0 International License. The images or other third party material in this article are included in the article's Creative Commons license, unless indicated otherwise in the credit line; if the material is not included under the Creative Commons license, users will need to obtain permission from the license holder to reproduce the material. To view a copy of this license, visit <http://creativecommons.org/licenses/by/4.0/>

© The Author(s) 2017